Electronic Supplementary Material (ESI) for Nanoscale.

Supplementary Information

Electrochemical Polymerization of Pyrene and Aniline Exclusively inside the Pores of Activated Carbon for High-Performance Asymmetric Electrochemical Capacitors

Hiroyuki Itoi,[*†] *Shintaro Maki,*[†] *Takeru Ninomiya,*[†] *Hideyuki Hasegawa,*[†] *Hidenori Matsufusa,*[†] *Shinya Hayashi,*[†] *Hiroyuki Iwata*[‡] *and Yoshimi Ohzawa*[†]

[†]Department of Applied Chemistry, and [‡]Department of Electrical and Electronics Engineering, Aichi Institute of Technology, Yachigusa 1247, Yakusa-cho, Toyota, 470-0392, Japan.

*E-mail: itoi-hiroyuki@aitech.ac.jp

1. Schematic illustration of electrode preparation and cell assemblies.

Fig. S1 shows the schematic illustration of the electrode preparation and cell assemblies.

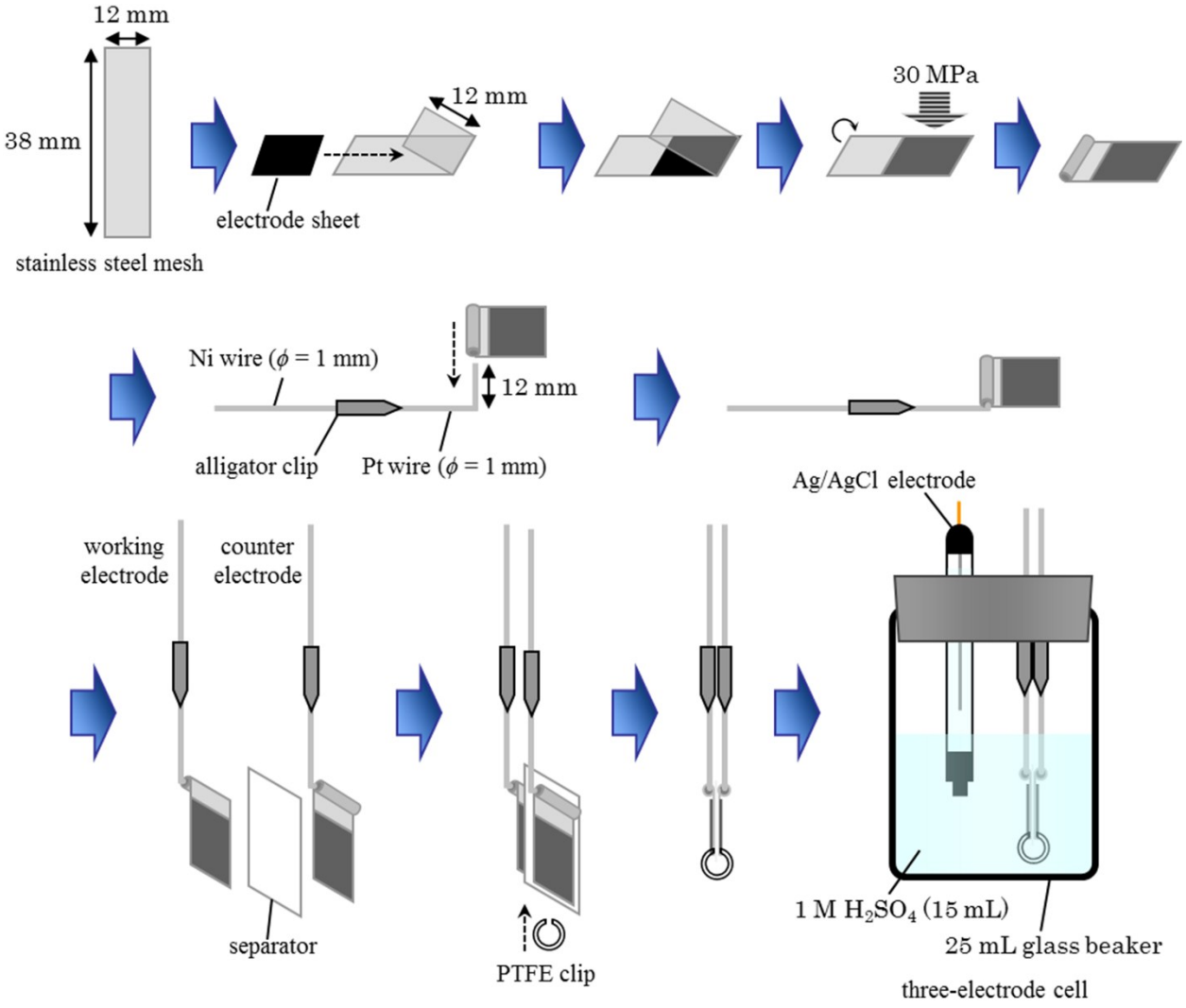

Fig. S1 Schematic illustration of the assemblies for the electrochemical cell.

1. Nitrogen adsorption/desorption isotherms and pore size distributions of the AC/PY and AC/ANI samples.

Fig. S2a and b show the adsorption/desorption isotherms for the AC/PY and AC/ANI samples, respectively. The result of AC is plotted together. BET SSAs and pore volumes of the samples are summarized in Table S1. As presented in the figure and Table S1, the surface areas and pore volumes of the AC/PY and AC/ANI samples decrease with the amount of the adsorbed monomers, and AC/PY (60.2%) and AC/ANI (62.4%) no longer have a surface area and pore volume, indicating that the pores of AC are completely filled with monomers.[1] Fig. S2c and d present the pore size distributions (PSDs) of the AC/PY and AC/ANI samples calculated by the non-local density functional theory (NLDFT) based on the models of N_2 @ 77K on carbon and slit pores with non-negative regularization method. The PSD of AC is also presented in the figure. It can be confirmed from the PSD of AC that AC has not only micropores but also mesopores less than 4 nm. On the other hand, the decrease in the pore volumes are clearly observed in the PSDs of the AC/PY and AC/ANI samples, indicating the pore filling with the monomers.

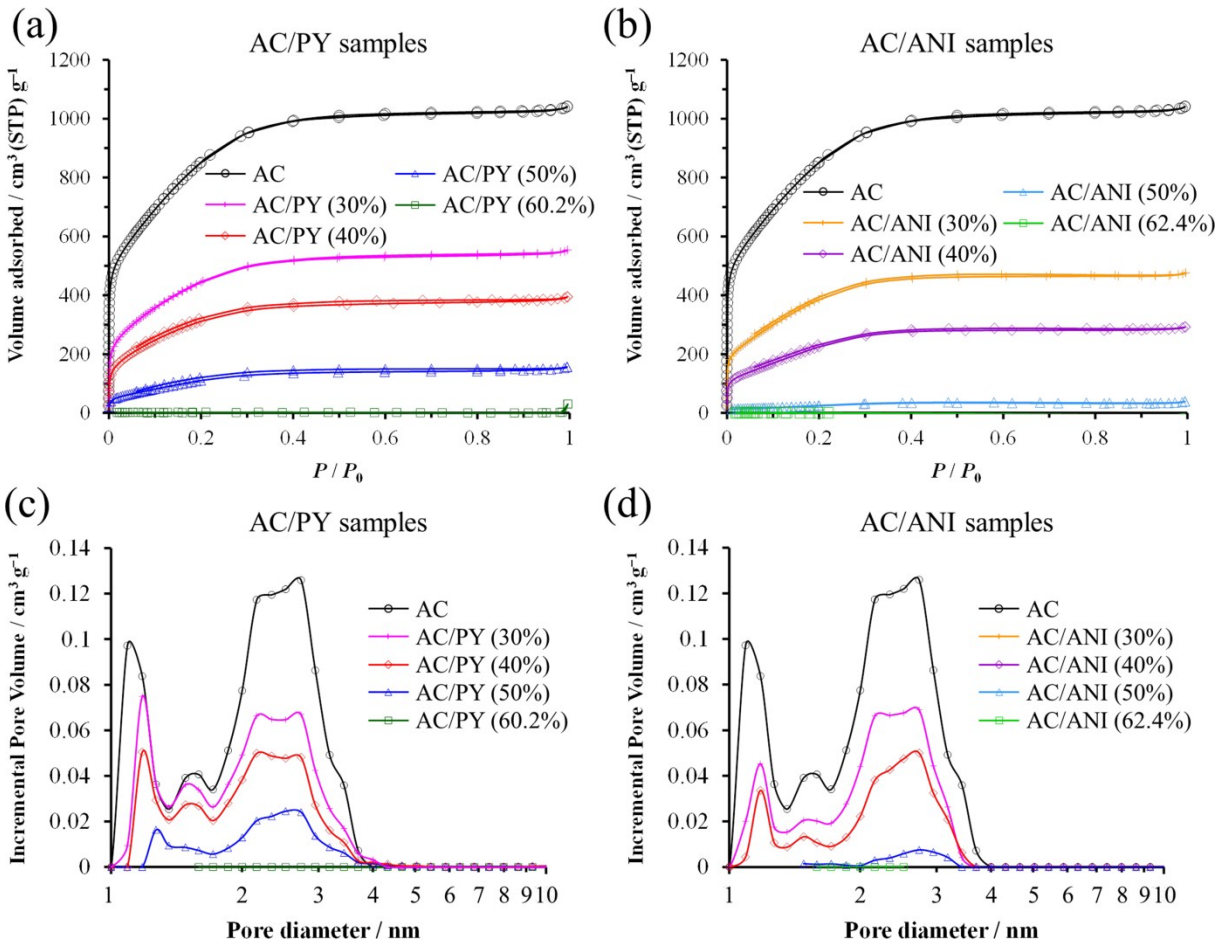

Fig. S2 (a,b) Nitrogen adsorption/desorption isotherms for (a) AC/PY and (b) AC/ANI samples. (c,d) PSDs of (a) AC/PY and (b) AC/ANI samples. The result of AC is also plotted together for comparison.

Table S1 The BET SSAs and pore volumes for the AC/PY and AC/ANI samples together with AC

sample	BET SSA	V_{total}	V_{micro}	V_{meso}
	(m^2 g^{-1})	(cm^3 g^{-1})	(cm^3 g^{-1})	(cm^3 g^{-1})
AC	3160	1.59	0.99	0.60
AC/PY (30%)	1670	0.84	0.52	0.32
AC/PY (40%)	1190	0.59	0.37	0.23
AC/PY (50%)	440	0.23	0.12	0.11
AC/PY (60.2%)	0	0.00	0.00	0.00
AC/ANI (30%)	1480	0.72	0.42	0.30
AC/ANI (40%)	870	0.44	0.24	0.20
AC/ANI (50%)	90	0.05	0.03	0.02
AC/ANI (62.4%)	0	0.00	0.00	0.00

2. X-ray diffraction (XRD) patterns of the AC/PY and AC/ANI samples.

The AC/PY and AC/ANI samples were analyzed with an XRD-6100 instrument (Shimadzu) with Cu Kα radiation (λ = 1.5418 Å) at an accelerating voltage of 30 kV and a current of 20 mA. Fig. S3 presents the XRD patterns of all the samples. As shown in the figure, AC does not show a carbon (002) diffraction due to its highly activated carbon structure. The AC/PY samples show broad peaks at around 11 and 24º while the AC/ANI samples show two broad peaks overlapping at around 19 and 26°. In addition, their peak intensities increase with the amount of PY or ANI in the samples. These broad peaks are indicative of the fine dispersion of adsorbate without agglomerations on the surface of AC particles.[1,2]

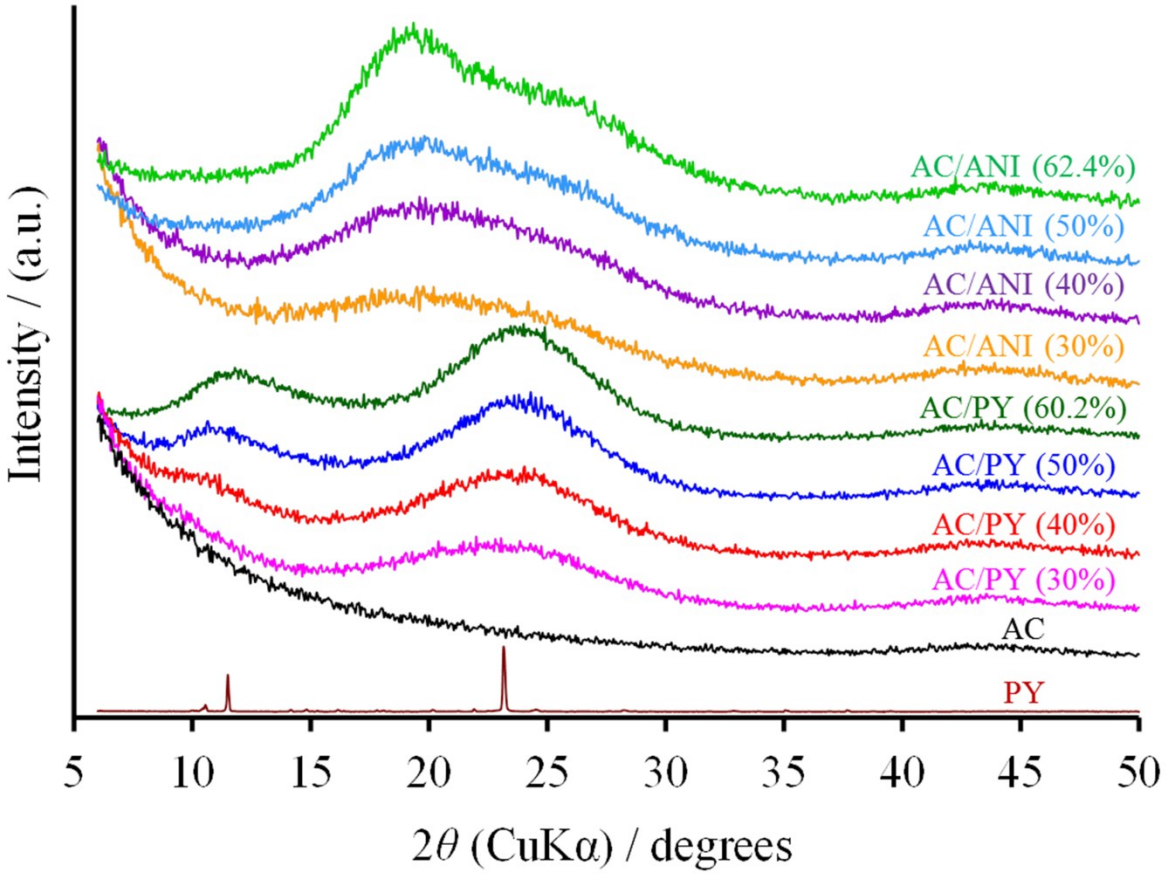

Fig. S3 XRD patterns of the AC/PY and AC/ANI samples. The XRD patterns of AC and PY are also presented for comparison.

3. Electrode densities.

The experimental electrode densities are summarized in Table S2.

Table S2 Experimental and theoretical electrode densities and electrode volumes per 1 g of AC

sample	density[a]	thoretical density[b]	electrode volume per 1 g of AC[c]
	ρ^{ex} (g cm^{-3})	ρ^{theo} (g cm^{-3})	V_{g-AC} (cm^3 g^{-1})
AC	0.326	–	3.41
AC/PY (30%)	0.447	0.452	3.44
AC/PY (40%)	0.515	0.522	3.45
AC/PY (50%)	0.613	0.620	3.44
AC/PY (60.2%)	0.792	0.768	3.31
AC/ANI (30%)	0.453	0.452	3.40
AC/ANI (40%)	0.506	0.522	3.51
AC/ANI (50%)	0.629	0.620	3.36
AC/ANI (62.4%)	0.808	0.813	3.43

[a] Experimental values.

[b] Theoretical values calculated from $\rho_{AC}^{ex}(90/(100-X)+0.1)$.

[c] Electrode volumes per 1 g of AC calculated from $1/W'_{AC}$.

4. Calculations for the theoretical electrode density and the electrode volume per 1 g of AC.

For the comparison with the experimental electrode density, a theoretical electrode density ($\rho^{theo}\ g\ cm^{-3}$) was determined using the experimental electrode density of AC ($\rho_{AC}^{ex}\ g\ cm^{-3}$) with the assumption that PY or ANI is adsorbed exclusively inside the pores of AC (Fig. S4a and b), where the AC particles do not expand after the adsorption of PY or ANI. As illustrated in Fig. S4, the weights of AC, monomer (PY or ANI), carbon black, and PTFE in 1 cm^3 of the electrode are denoted as $W_{AC}(=0.9\rho_{AC}^{ex})$, $W_{mono}(=0.9\rho_{AC}^{ex}X/(100-X))$, $W_{CB}(=0.05\rho_{AC}^{ex})$, and $W_{PTFE}(=0.05\rho_{AC}^{ex})$, respectively, and ρ^{theo} is calculated from the following equation,

$$\rho^{theo}=\rho_{AC}^{ex}\left(\frac{90}{100-X}+0.1\right)$$

where, X is the weight percent of the monomer in the sample. The theoretical electrode densities are also summarized in Table S2. As shown in Table S2, the experimental electrode densities are

good agreement with the theoretical values, indicating that there are little PY or ANI molecules on the particle surfaces of AC.

From the experimental electrode density (ρ^{ex}) and the weight percent of the monomer in the sample (X), the electrode volume per 1 g of AC ($V_{g-AC}\, cm^3\, g_{AC}^{-1}$) can be determined. First, the actual weight of AC in 1 cm^3 of the electrode ($W'_{AC}\, g$), which is not a theoretical value as illustrated in Fig. S4, is calculated from the following equation,

$$W'_{AC} = \rho^{ex} \times \frac{18}{18 + \frac{18X}{100 - X} + 1 + 1} = \frac{9\rho^{ex}}{10 + \frac{9X}{100 - X}}$$

Thus, V_{g-AC} is calculated as the reciprocal of W'_{AC} ($= 1/W'_{AC}$). The V_{g-AC} values for the AC/PY and AC/ANI samples are also summarized in Table S2.

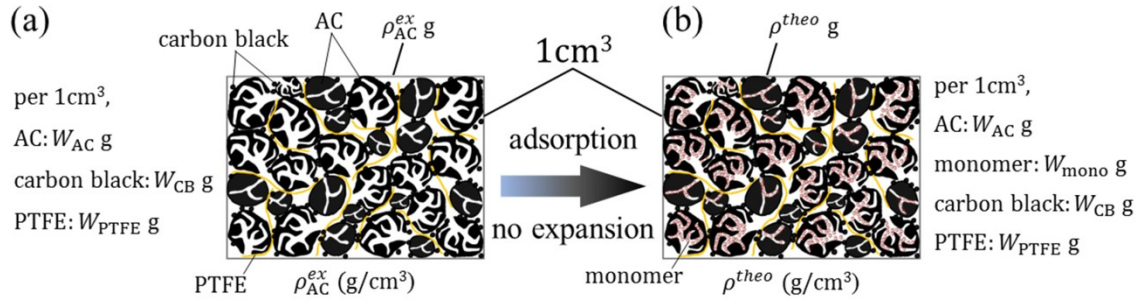

$W_{AC}: W_{CB}: W_{PTFE} = 18:1:1$

$W_{AC} = 0.9\rho_{AC}^{ex}$

$W_{CB} = W_{PTFE} = 0.05\rho_{AC}^{ex}$

$\rho_{AC}^{ex} = W_{AC} + W_{CB} + W_{PTFE}$

$W_{AC}: W_{CB}: W_{PTFE} = 18:1:1$, $W_{AC}: W_{mono} = (100 - X): X$

$W_{AC}: W_{mono}: W_{CB}: W_{PTFE} = 18: \frac{18X}{100 - X}: 1:1$

$W_{AC} = 0.9\rho_{AC}^{ex}$, $W_{CB} = W_{PTFE} = 0.05\rho_{AC}^{ex}$

$W_{mono} = 0.9\rho_{AC}^{ex} \frac{X}{(100 - X)}$

$\rho^{theo} = W_{AC} + W_{mono} + W_{CB} + W_{PTFE} = \rho_{AC}^{ex}\left(\frac{90}{100 - X} + 0.1\right)$

Fig. S4 Schematic illustration of the electrodes prepared in this study. (a) The electrode consisting of AC, carbon black (CB), and PTFE. (b) The electrodes of the AC/PY and AC/ANI samples. The theoretical density is calculated assuming that the carbon particles do not expand upon the adsorption of the monomer (PY or ANI) and its subsequent polymerization, where W_{AC}, W_{CB}, and W_{PTFE} are constant for all the electrodes, respectively.

As shown in Table S2, ρ^{ex} increases with the amount of the monomer in the sample and is in good agreement with ρ^{theo}. Moreover, V_{g-AC} holds a nearly constant value for each sample, indicating that the electrode volume does not expand upon the adsorption of the monomers. These results suggest that there are very few PY or ANI molecules on the AC particles. Furthermore, the absence of PPY or PANI on the AC particles was directly confirmed by the SEM and TEM observations (Fig. 2).

The gravimetric capacitance (C_g) was calculated on the basis of the mass of the active material (*i.e.*, the weight of AC and monomer), while the volumetric capacitance (C_v) was calculated on the basis of the volume including AC, monomer, carbon black, and PTFE. Therefore, C_v is calculated based on the above discussion by using the following equation,

$$C_v = C_g \times \rho^{ex} \times \frac{18 + \frac{18X}{100 - X}}{\frac{18X}{100 - X} + 1 + 1} = C_g \frac{900\rho^{ex}}{1000 - X}$$

5. Cyclic voltammograms for electrochemical polymerization.

Fig. S5 shows the cyclic voltammograms for the electrochemical polymerizations of the AC/PY and AC/ANI samples. A large irreversible anodic current is observed between 0.9 and 1.2 V for the AC/PY samples and 0.7 and 1.0 V for the AC/ANI samples, respectively. The irreversible current decreases with the number of cycles, while the reversible anodic and cathodic peaks appear and their peak currents increase with the number of cycles. Both anodic and cathodic peak currents reached maximum values after the 15th cycle. These results indicate that the irreversible currents are derived from the polymerization of the monomers and the polymerization reactions complete after ca. 15 cycles, while the anodic and cathodic currents are derived from the redox reactions of PPY and PANI.

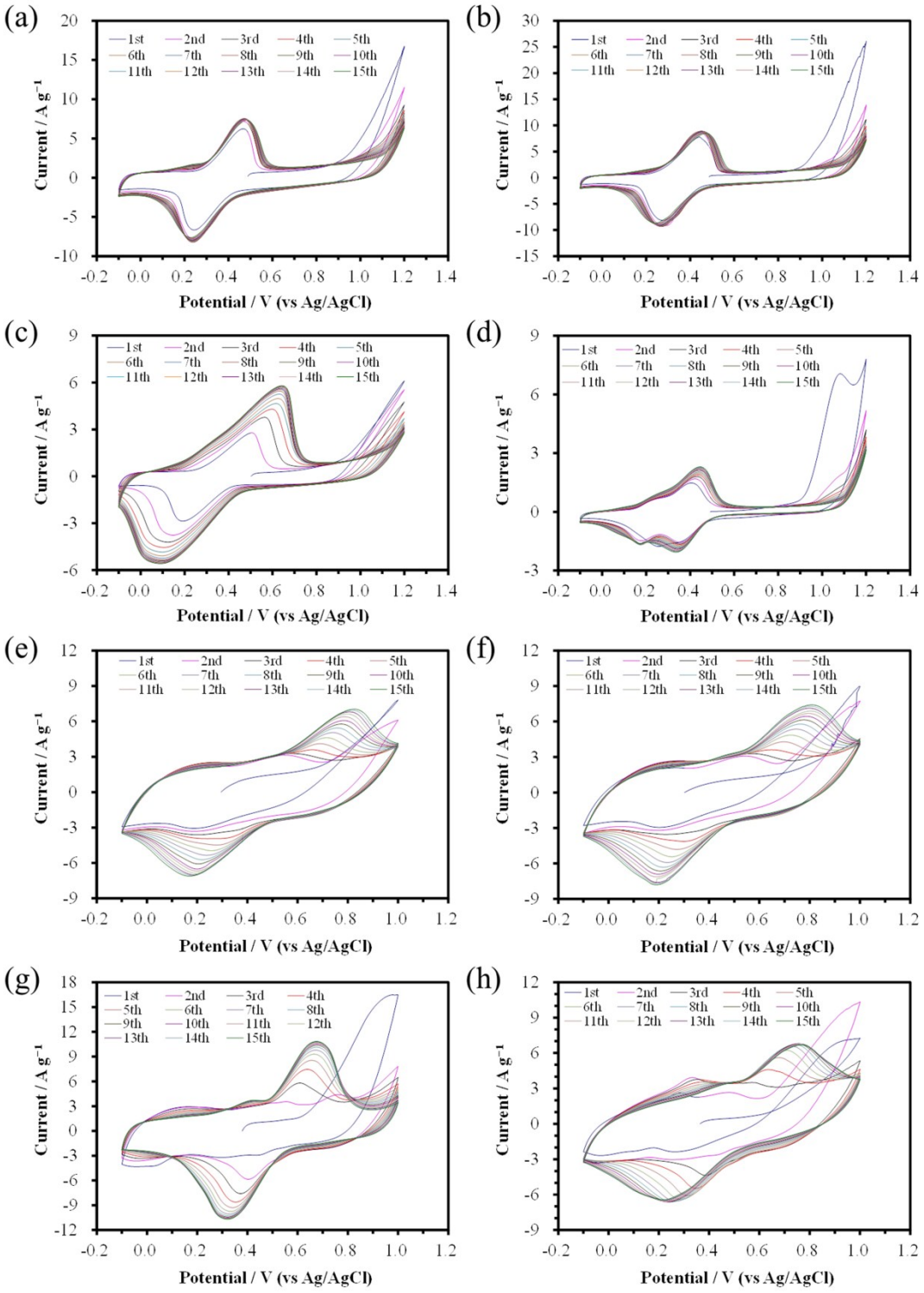

Fig. S5 Cyclic voltammograms for the electrochemical polymerization of (a) AC/PY (30%), (b) AC/PY (40%), (c) AC/PY (50%), (d) AC/PY (60.2%), (e) AC/ANI (30%), (f) AC/ANI (40%), (g) AC/ANI (50%), and (h) AC/ANI (62.4%).

6. Geometry optimization.

The geometry optimization was performed with density functional theory (DFT) calculation using B3LYP functional coupled with the 6-31G basis set. Fig. S6 shows the geometry optimized structures of ANI, PY, and 1,1-bipyrene.

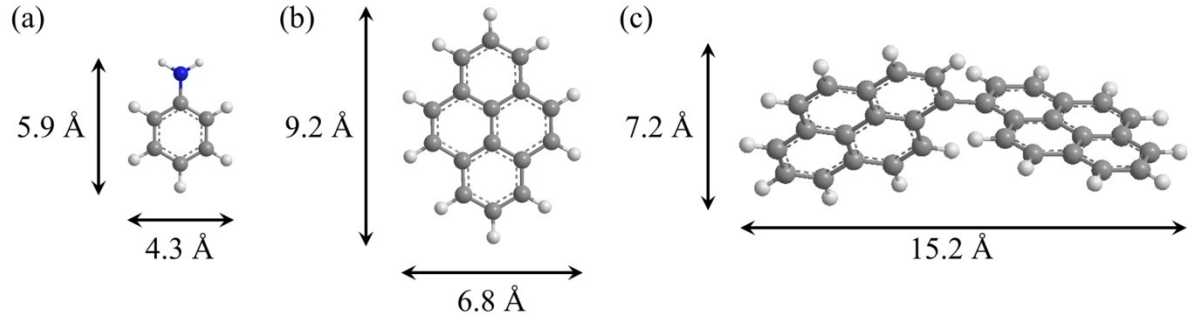

Fig. S6 Geometry optimized structures of (a) ANI, (b) PY, and (C) 1,1'-bipyrene.

7. Reactions of the electrochemical polymerization of PY.

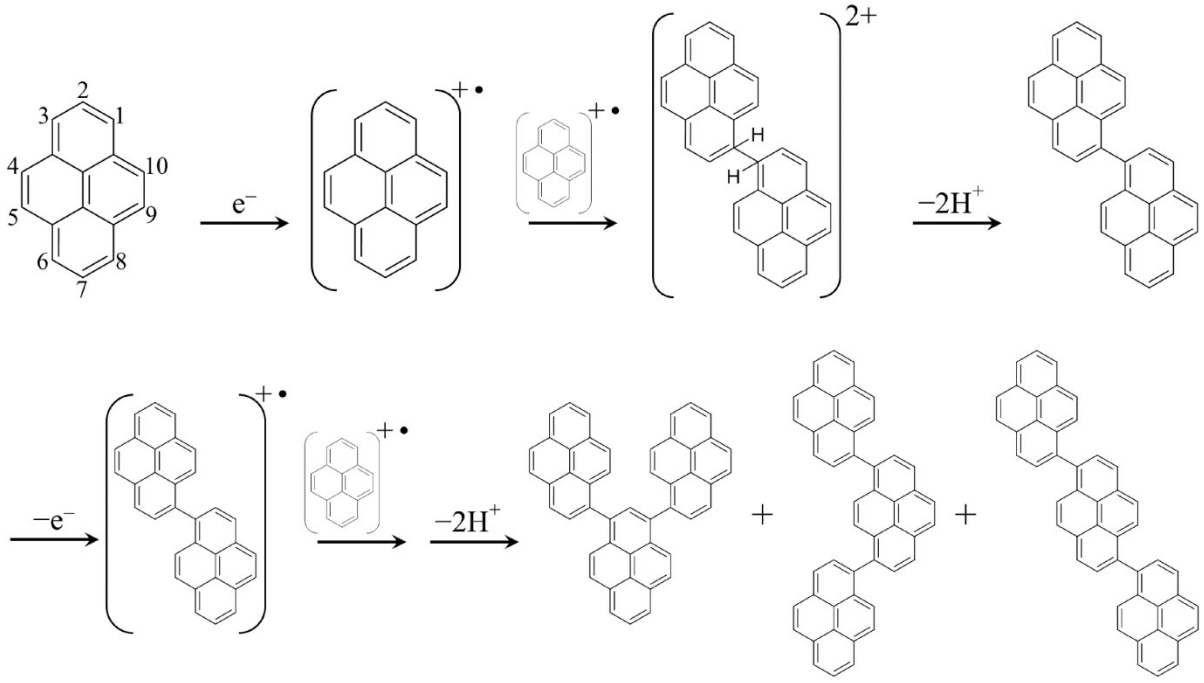

Fig. S7 A possible reactions of the electrochemical polymerization of PY.

8. Scanning electron microscope (SEM) images of carbon black and PTFE.

Fig. S8a and b show carbon black. The fine particles observed in Fig. 2a−c are carbon black particles. The SEM images of PTFE are shown in Fig. S8c and d.

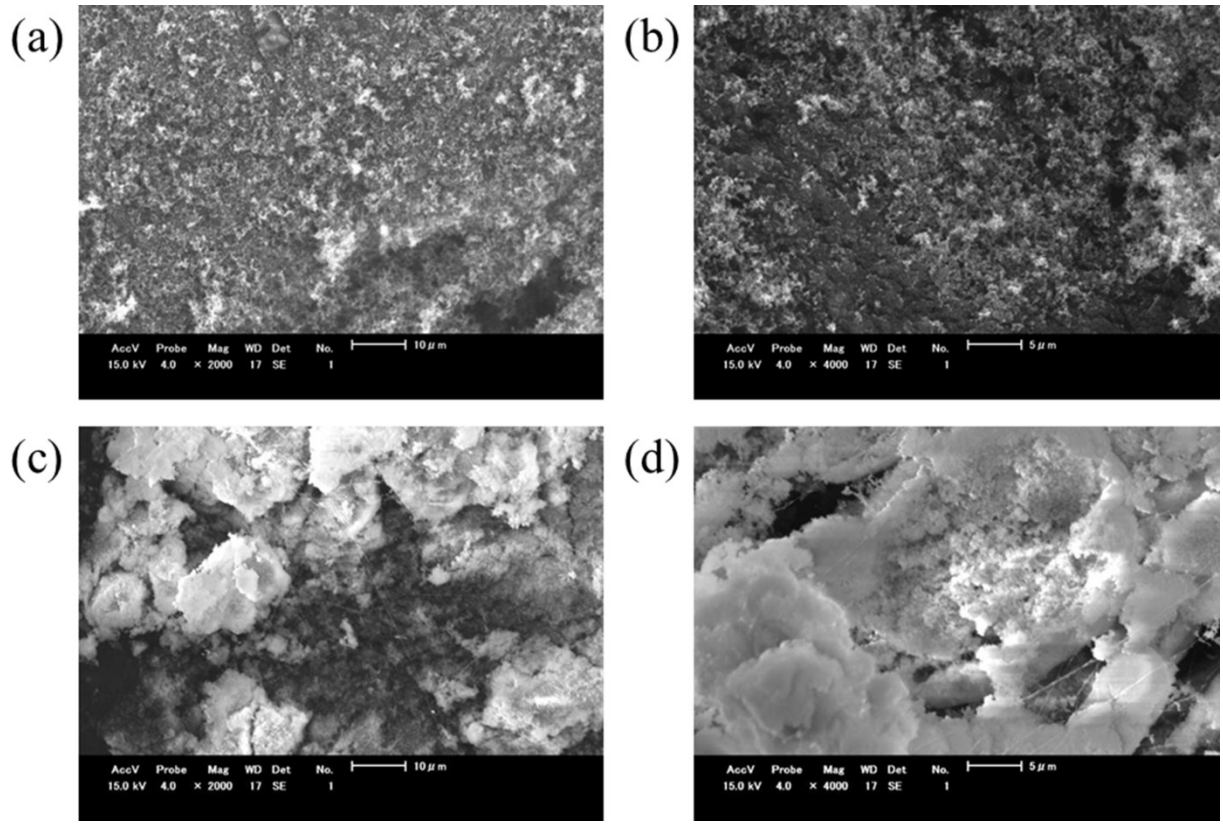

Fig. S8 SEM images of (a,b) carbon black and (c,d) PTFE.

9. Comparison of the XRD patterns between the electrodes before and after electrochemical polymerization.

The electrodes after polymerization were washed with a plenty of deionized water with stirring for 24 h after electrochemical polymerization, followed by being dried at 60 ºC under vacuum for 12 h. The XRD patterns for the electrode sheets of AC/PY (50%), AC/ANI (50%), AC/PPY (50%), and AC/PANI (50%) are shown together with AC/PY (50%) and AC/ANI (50%) in Fig. S9. AC/PPY (50%) and AC/PANI (50%) showed the most excellent electrochemical capacitor performance among the AC/PPY and AC/PANI samples, respectively. The XRD patterns of carbon black and PTFE, which were used to prepare the electrodes, are plotted together. As shown in the figure, the XRD patterns for the electrodes of AC/PY (50%) and AC/ANI (50%) before the electrochemical polymerization show the similar peaks to those of AC/PY (50%) and AC/ANI (50%) except the existence of the peaks of carbon black and PTFE, which locate at 26 and 43º derived from carbon (002) and (10) diffraction planes for carbon black and 18º for PTFE, respectively. After the polymerization, the broad peak at around 24° observed for AC/PY (50%) shifted to higher angle, while the broad peaks at 19 and 26° observed for AC/ANI (50%) decreased and increased, respectively. AC/PPY (50%) and AC/PANI (50%) exhibited no distinct peaks characteristic of bulk polymers.[3] These results suggest that PPY and PANI in the samples have a very thin structure because they were synthesized not onto the surfaces of the AC particles but inside the pores of AC.[2] This was evidenced by XPS analysis and TEM observation (Fig. 1 and 2).

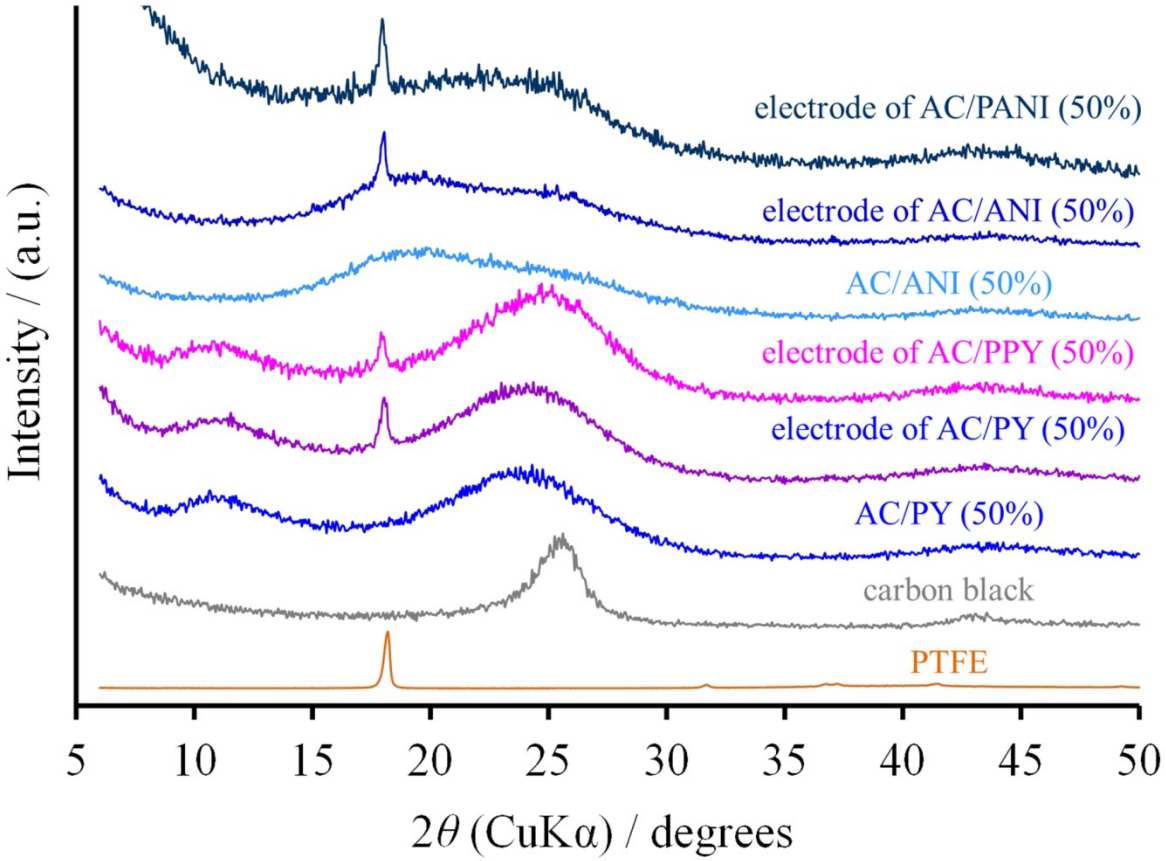

Fig. S9 XRD patterns for the electrodes of AC/PY (50%), AC/ANI (50%), AC/PPY (50%), and AC/PANI (50%). The XRD patterns of AC/PY (50%), AC/ANI (50%), carbon black, and PTFE are also plotted together.

10. Nitrogen adsorption/desorption isotherms of the electrodes for AC/PANI (62.4%) just after the electrochemical polymerization and after the GC analysis.

The electrodes of AC/PANI (62.4%) just after the electrochemical polymerization and after the GC analysis were measured by nitrogen adsorption/desorption analysis. The electrodes were washed with a plenty of deionized water with stirring for 24 h, followed by being dried at 60 ºC under vacuum for 12 h. Before the analysis, the electrodes were dried at 100 °C under vacuum for 6 h. The BET surface areas of the electrodes just after the CV polymerization and GC analysis were 1140 and 1220 $m^2\ g^{-1}$, respectively. The error estimated from the repeatability of the measured values for BET SSA is within 10 $m^2\ g^{-1}$.

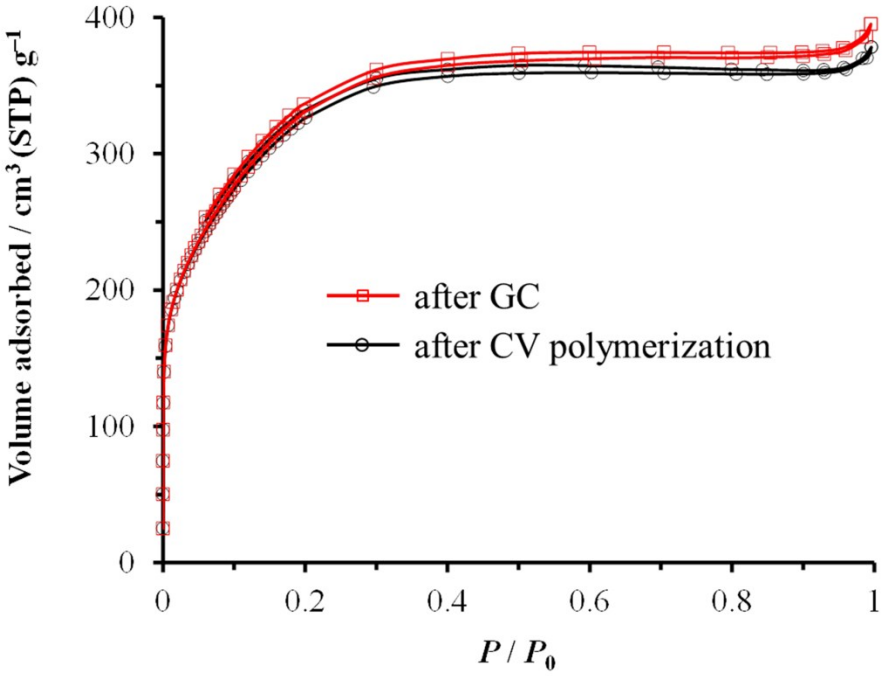

Fig. S10 Nitrogen adsorption/desorption isotherms of the electrodes for AC/PANI (62.4%) just after the electrochemical polymerization and after the GC analysis.

11. Cyclic voltammetry of the counter electrodes for AC/PPY (60.2%) and AC/PANI (62.4%).

The counter electrodes of AC/PPY (60.2%) and AC/PANI (62.4%) were analyzed with CV after the GC analysis to confirm the desorption of PPY or PANI from AC. The voltammograms were collected at 1 mV s^{-1} in a potential range of −0.1 to 0.8 V. As presented in Fig. S11, the redox peaks derived from PANI are observed for the counter electrode of AC/PANI (62.4%) while no distinct redox peak corresponding to PPY was observed for the counter electrode of AC/PPY (60.2%).

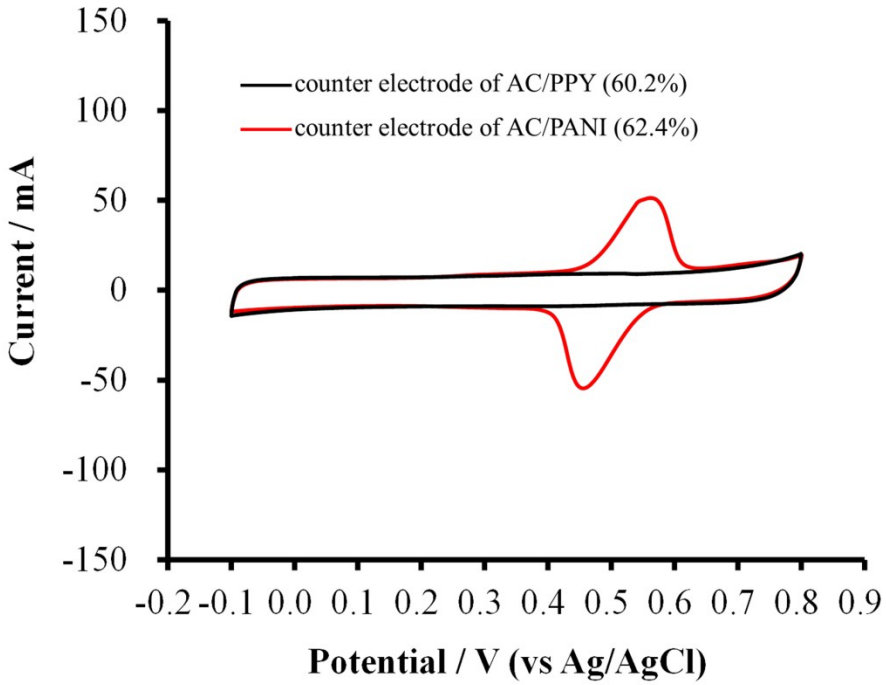

Fig. S11 The voltammograms of the counter electrodes of AC/PPY (60.2%) and AC/PANI (62.4%) after the GC analysis.

12. Comparison between R_s and electrochemical performances.

The electrochemical performances of AC/PPY (50%) were measured by using three different cells (cell A−C). The measurements were performed by using a three-electrode cell in the same manner as described in the manuscript. Three cells were prepared independently from AC/PY (50%) and electrochemical performances were measured after the electrochemical polymerization of PY. As shown in Fig. S12a, three cells exhibited almost the same size of the semicircle and a vertical line but showed the different R_s (*i.e.*, the intersection of the Nyquist plots in the highest-frequency region and the real axis). However, the capacitance retentions of the cell A, B, and C at 10 A g^{-1} were 88, 86, and 85%, respectively, relative to their capacitances at 0.1 A g^{-1} (Fig. S12b). Thus, there is almost no difference in the rate capabilities of these three cells, suggesting that R_s has nothing to do with the rate capability (*i.e.*, power density) of the samples.

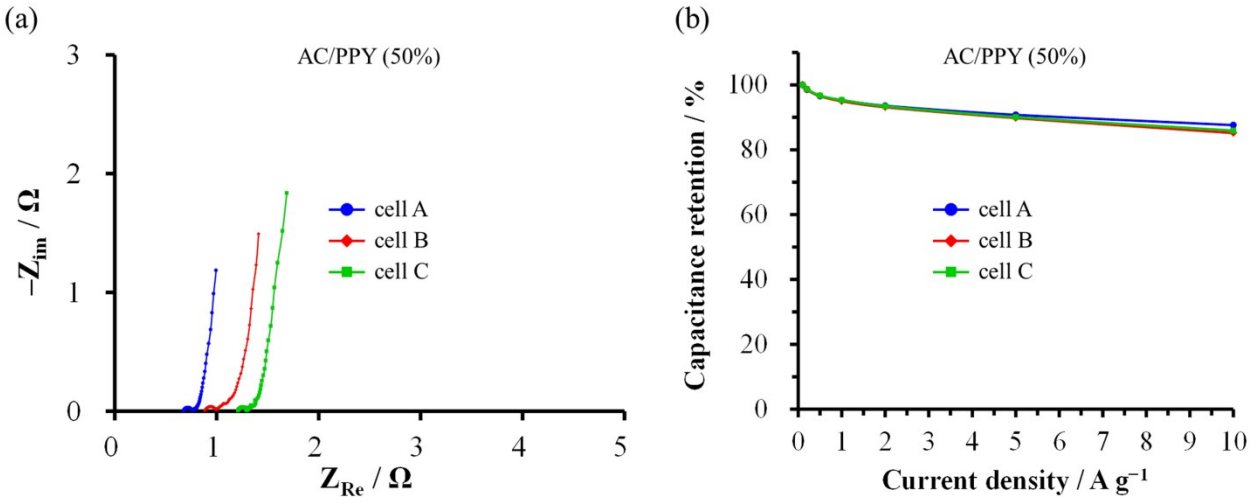

Fig. S12 (a) Nyquist plots and (b) capacitance retentions of the three different cells prepared from AC/PY (50%). The electrochemical cells were prepared independently by using AC/PY (50%).

13. Fitting of Nyquist plots.

Fig. S13 shows the Nyquist plots for the AC/PPY and AC/PANI samples and their fitting data. The results of R_{ct} were summarized in Table S3.

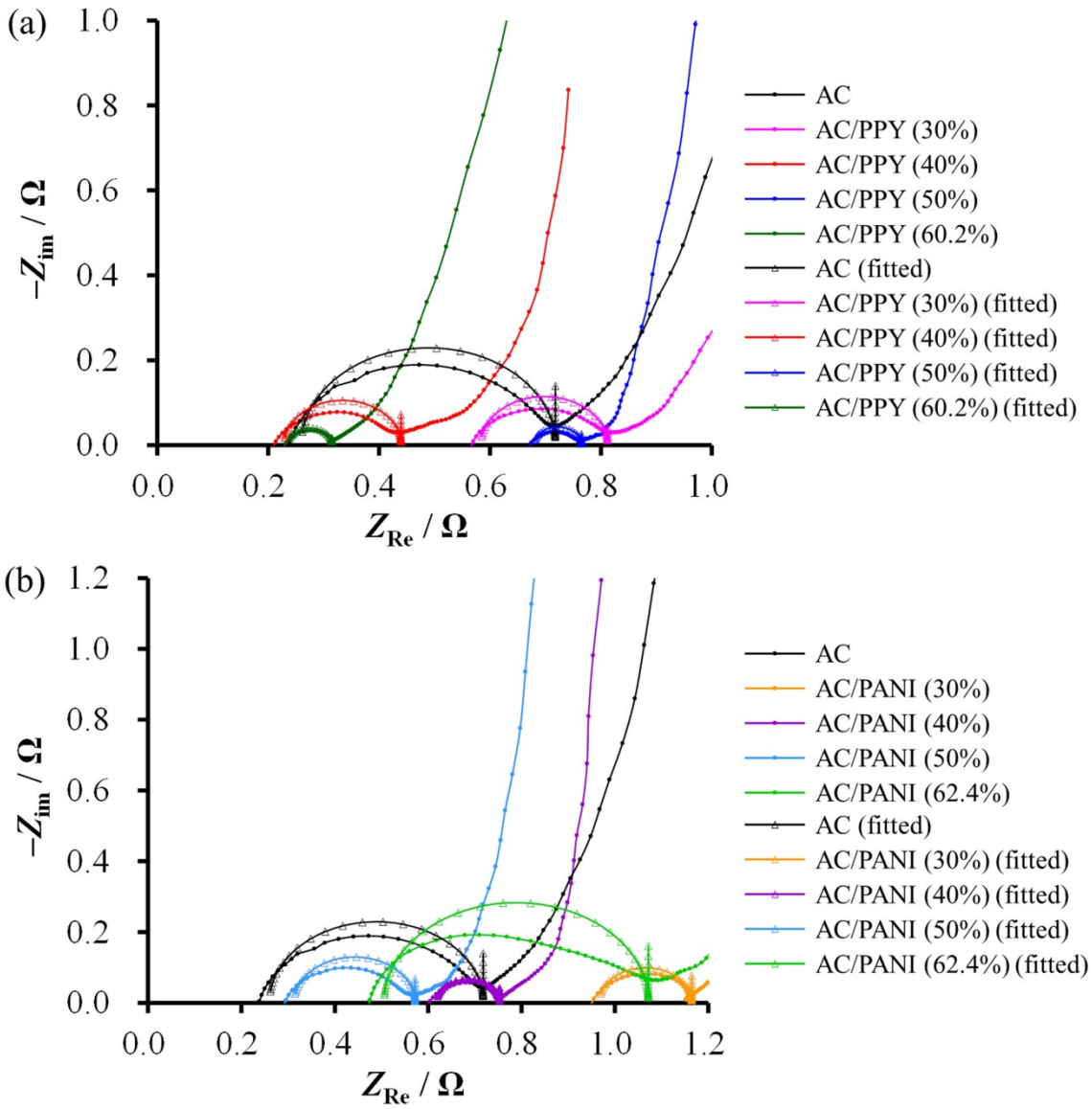

Fig. S13 Nyquist plots and fitted data for (a) AC/PPY and (b) AC/PANI samples, shown alongside the data of AC. The Nyquist plots of the AC/PPY and AC/PANI samples were collected at the potentials of their oxidation peak maxima. The Nyquist plot of AC was collected at 0.4 V.

Table S3 summarizes the R_{ct} of the AC/PPY, AC/PANI, and AC samples. The capacitances of AC/PPY (50%) and AC/PANI (50%) strongly depended on the pseudocapacitance, while R_{ct} of AC/PPY (50%) is smaller than that of AC/PANI (50%). This result indicates that PPY has higher electrical conductivity than PANI.

Table S3 R_{ct} of the AC/PPY and AC/PANI samples together with AC

sample	R_{ct} (Ω)
AC	0.46
AC/PPY (30%)	0.23
AC/PPY (40%)	0.21
AC/PPY (50%)	0.09
AC/PPY (60.2%)	0.08
AC/PANI (30%)	0.20
AC/PANI (40%)	0.14
AC/PANI (50%)	0.26
AC/PANI (62.4%)	0.57

REFERENCES

(1) Itoi, H.; Yasue, Y.; Suda, K.; Katoh, S.; Hasegawa, H.; Hayashi, S.; Mitsuoka, M.; Iwata, H.; Ohzawa, Y. Solvent-free Preparation of Electrochemical Capacitor Electrodes Using Metal-free Redox Organic Compounds. *ACS Sustainable Chem. Eng.* **2017**, *5*, 556−562.

(2) Itoi, H.; Hayashi, S.; Matsufusa, H.; Ohzawa, Y. Electrochemical Synthesis of Polyaniline in the Micropores of Activated Carbon for High-Performance Electrochemical Capacitors. *Chem. Commun.* **2017**, *53*, 3201−3204.

(3) Hu, Z.; Zu, L.; Jiang, Y.; Lian, H.; Liu, Y.; Li, Z.; Chen, F.; Wang, X.; Cui, X. High Specific Capacitance of Polyaniline/Mesoporous Manganese Dioxide Composite Using KI-H_2SO_4 Electrolyte. *Polymers* **2015**, *7*, 1939−1953.